Piezostrain-controlled magnetization compensation temperature in ferrimagnetic GdFeCo alloy films

Junshuai Wang,[1] Mingfen Li,[2] Chaozhong Li,[1] Rujun Tang,[3] Mingsu Si,[2] Guozhi Chai,[1] Jinli Yao,[1] Chenglong Jia,[1,*] and Changjun Jiang[1,*]

[1]*Key Laboratory for Magnetism and Magnetic Materials of Ministry of Education, Lanzhou University, Lanzhou 730000, People's Republic of China*

[2]*School of Materials and Energy, Lanzhou University, Lanzhou 730000, People's Republic of China*

[3]*Jiangsu Key Laboratory of Thin Films, School of Physical Science and Technology, Soochow University, Suzhou 215006, People's Republic of China*

(Received 6 November 2022; revised 27 April 2023; accepted 28 April 2023; published 11 May 2023)

The electrical control of magnetization compensation temperature (T_{com}) is investigated in ferrimagnetic GdFeCo alloy deposited on ferroelectric $Pb(Mg_{1/3}Nb_{2/3})O_3$-30%$PbTiO_3$ (PMN-PT). It is found that the applied electric field can cause a 19 K shift in T_{com}. T_{com} under different applied electric fields across the PMN-PT substrate suggests that such electrical control is induced by piezostrain at the ferroelectric-ferrimagnetic interface. Spin-polarized first-principles calculations show that the change of exchange coupling strength in GdFeCo are caused by the lattice strains. Nonvolatile switching of resistance and direct bipolar control of exchange bias are achieved when an electric field is applied to appropriately designed multilayers. Our findings pave the way for electric field control of T_{com} in ferrimagnetic GdFeCo alloy and have implications for the development of energy efficient and nonvolatile ferrimagnetic magnetic random access memory.

DOI: 10.1103/PhysRevB.107.184424

I. INTRODUCTION

Spintronic devices, such as magnetic tunnel junctions (MTJs), are a hot topic in information storage device research due to their potential for low power consumption, nonvolatility, high storage density, and fast operation [1–4]. Ferromagnet (FM)-based MTJs were widely studied for magnetic random access memory (MRAM) applications and have been commercialized recently [5–8]. Ferrimagnets (FIMs) have several advantages over FMs, including faster writing speed and higher storage density due to FIMs' ultrafast (THz) spin dynamics [8], antiparallel-aligned unbalanced multisublattice magnetization [9], and existence of bulk perpendicular magnetic anisotropy [10,11]. Zhao *et al.* [12] and Cao *et al* [13] demonstrated field-free spin-orbit torque (SOT)-induced deterministic magnetization switching in a single FIM CoTb alloy, which was introduced by the vertical structural inversion asymmetry due to the composition gradient of CoTb alloy or the in-plane magnetization of attached Co films [14,15]. Compared to FMs [12], the efficiency of field-free SOT-induced switching in FIMs can be significantly increased, promoting the use of FIMs in MRAMs with tunneling magnetoresistance readout [13]. However, SOT generation is accompanied by the induction of a high-density in-plane charge current [16–18]. The Joule heat of charge currents would reduce the thermal stability of device and increase energy consumption [8,19].

Alongside SOT-induced magnetization switching in FIM alloys, electric fields (E) were also used to control the magnetic moment and achieve *in situ* 180° magnetization reversal in the FIM GdCo alloy [20]. The use of electric field rather than charge current can significantly lower power consumption and avoid Joule heating in the devices [21]. Beach *et al.* achieved a large modulation (∼100 K) of magnetization compensation temperature (T_{com}) and a 180° switching of the net magnetization in $GdCo/Pd/GdO_x$ heterostructures by introducing gate voltage through the injection of hydrogen into the GdCo alloy. However, electrical 180° switching of the magnetization involved the hydrolysis of water in ambient moisture and happened only when the water vapor was present in the gas environment. Furthermore, the water vapor can cause chemical reactions with heterostructures rendering the resistance state of the latter volatile, which does not meet the requirement of nonvolatile magnetoelectric random access memory (ME-RAM) [22–24].

In this study, we demonstrate electric field-controlled magnetization compensation temperature in an amorphous rare-earth (RE)-transition metal (TM) FIM GdFeCo alloy. A typical butterflylike T_{com}-E curve implies that the switching is closely related to the piezostrain-mediated magnetoelectric (ME) coupling in ferroelectric (FE)-FIM heterostructures. Spin-polarized first-principles calculations show that the strength of exchange coupling in the GdFeCo alloy can indeed be modulated by strains. Under isothermal conditions, nonvolatile and reversible switching of resistance is observed, indicating stable and reversible "ON"-"OFF" switching behavior. Furthermore, E-controllable exchange bias and nonvolatility are also achieved in appropriately

*Author to whom correspondence should be addressed: cljia@lzu.edu.cn; jiangchj@lzu.edu.cn

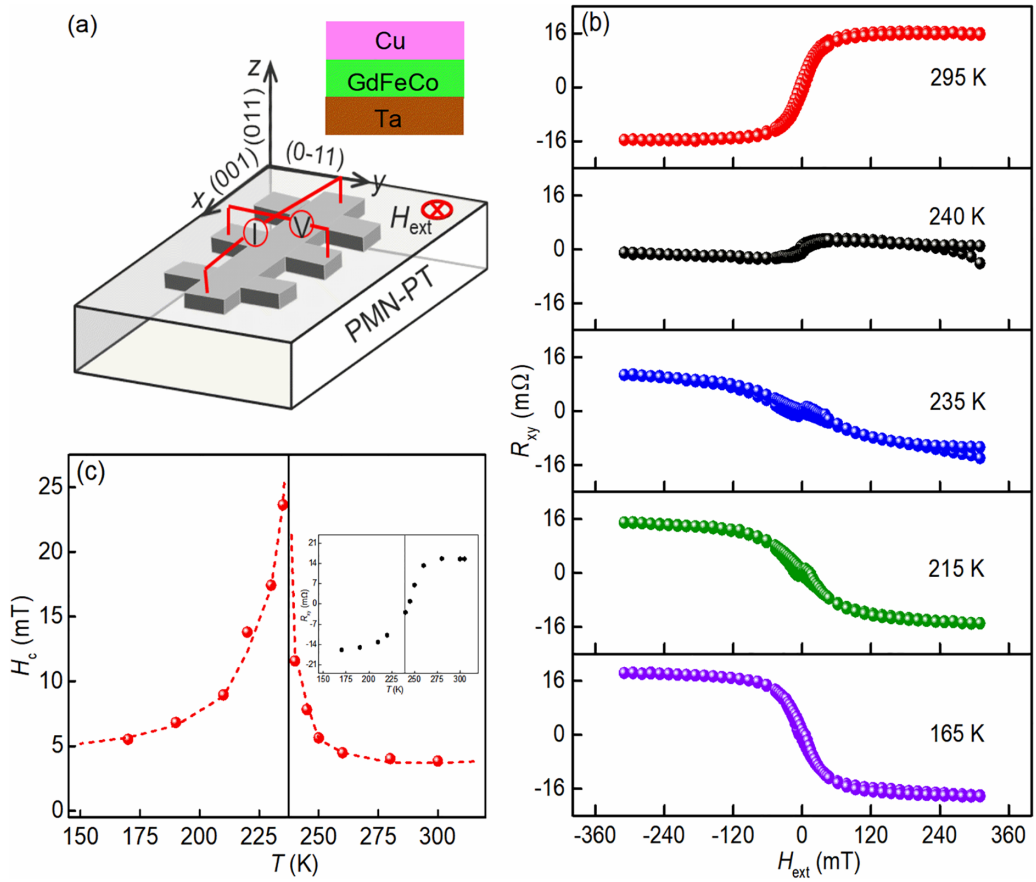

FIG. 1. (a) Schematic view of the Ta/GdFeCo/Cu heterostructure with Hall bar structure and measurement setup. Current is applied along the x direction and the Hall resistance is measured along the y direction. (b) Hall resistance as a function of magnetic field at different temperatures (from 165 to 295 K). (c) Coercivity extracted from the hysteresis loops of heterostructures versus temperature. The inset shows saturation resistance of the heterostructure measured at 310 mT as a function of temperature.

designed multilayers. Our findings hold great promise for implementation in devices such as nonvolatile ME-RAMs, as well as for understanding the effect of piezostrain on the magnetic properties of FIM materials.

II. EXPERIMENTAL SETUP

Ta (5 nm)/$Gd_{29}Fe_{51}Co_{20}$ (5 nm)/Cu (5 nm) heterostructures were deposited on 400-μm (011)-oriented single-crystalline $Pb(Mg_{1/3}Nb_{2/3})O_3$-30%$PbTiO_3$ (PMN-PT) substrates at room temperature by dc magnetron sputtering with a base pressure below 2.0×10^{-5} Pa. Ta films were deposited onto the PMN-PT substrates as buffer layers to reduce the influence of substrate roughness. GdFeCo films were formed by depositing GdFeCo alloy targets. Cu capping layers were deposited as top electrodes and to protect GdFeCo alloy from oxidation. The PMN-PT/Ta (5 nm)/$Gd_{29}Fe_{51}Co_{20}$ (5 nm)/IrMn (15 nm)/Cu (5 nm) structure was deposited to study exchange bias. To ensure the pinning direction coincided with the growth direction of heterostructure layers, a constant magnetic field of about 315 mT was applied along this direction during growth. Maskless exposure technique was used to pattern these layers into Hall bar devices ($300 \times 2000\,\mu m^2$) for the anomalous Hall effect (AHE) measurements, as shown in Fig. 1(a). During the temperature-dependent AHE measurements, the Hall bar devices were placed in vacuum thermostat (Model: LanHai Instrument-101C) at a base pressure below 10^{-3} Pa. Data was collected by connecting the thermostat wiring device to the test equipment (Keithley 2400-C Source Meter and Keysight 34420A Nano Volt/Micro Ohm Meter). Cu electrode with the thickness of 50 nm was deposited on the bottom of PMN-PT substrate as the electrode. An electric field using Keithley 6517 B dc power supply was applied perpendicularly to the PMN-PT substrate. Magnetic domains under electric field were investigated at 214 K using the polar magneto-optical Kerr effect (MOKE) (Model: Evico magnetics BmbH).

III. RESULTS AND DISCUSSIONS

A. Electric field modulation mechanism

Figure 1(b) shows the anomalous Hall resistance (R_{xy}) as a function of out-of-plane magnetic field at different temperatures to obtain T_{com} of Cu/$Gd_{29}Fe_{51}Co_{20}$/Ta heterostructures. The loops polarity from 295 to 240 K shows the same sign whereas below 240 K the loop polarity reversal. The reversal of the loop polarity between 240 and 235 K indicates that there exists T_{com} at which the net magnetization converges to zero. Because the Gd 4f electrons are far below the Fermi level, the R_{xy} is mostly sensitive to magnetic moments in the FeCo sublattice [3,20]. The net magnetization is dominated by

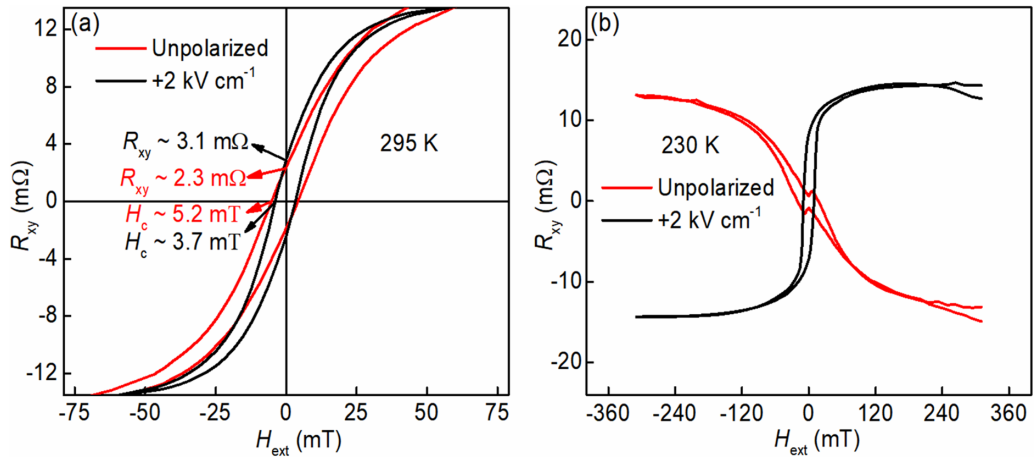

FIG. 2. Influence of electric field on R_{xy} of GdFeCo film. (a) and (b) show electric field-modulated AHE hysteresis loops for Cu/GdFeCo/Ta/Pb($Mg_{1/3}Nb_{2/3}$)O_3-30%$PbTiO_3$ (PMN-PT) heterostructures at ambient temperature and at 230 K, respectively.

the antiparallel spontaneous magnetization of Gd and FeCo below and above T_{com} (∼237 K), respectively. Figure 1(c) shows temperature dependence of coercivity (H_c). Here, the coercivity is defined as H_c=(H_{c+}-H_{c-})/2, where H_{c+} and H_{c-} are the coercivities for the ascending and descending branches of AHE loop, respectively. The extraction of H_{c+} and H_{c-} at small magnetic field range is shown in Fig. S1 in the Supplemental Material [25] (see also Refs. [26,27] therein) for details. The divergence of H_c is observed at T_{com} because a larger magnetic field is required to generate a sufficiently high Zeeman energy to switch the magnetization [11,28]. The inset of Fig. 1(c) shows the saturation R_{xy} as a function of temperature in the presence of positive magnetic fields, extracted from Fig. 1(b). The sign change of saturation R_{xy} near 240 K also indicates T_{com} of the heterostructures [9,11].

Figure 2(a) shows the AHE resistance loops of the heterostructure in the unpolarized (the initial state of the heterostructures) and positively polarized (by gate electric field +2 kV cm^{-1}) states at ambient temperature. The basic building blocks of the electric field control setup are schematically shown in Fig. S2 in the Supplemental Material [25] for details. To ensure the stability of measurements, the heterostructures were polarized several times before the measurements by applying different positive and negative electric fields. Compared with the value of R_{xy} in the unpolarized state (red line in the corresponding hysteresis loop), a large modulation (∼35%) at zero magnetic field (remanent R_{xy}) was induced by the applied +2 kV cm^{-1} electric field. The coercivity of heterostructures, on the other hand, is found to be decreased (∼40%) from approximately 5.2 to 3.7 mT by the electric field of +2 kV cm^{-1}. These large modulations could be attributed to the change of magnetic domain structures induced by external electric fields [29]. Figure 2(b) shows the AHE resistance loops of the heterostructure measured in 230 K at $E = 0$ (red line) and $E = +2$ kV cm^{-1} (black line). It shows that the electric field reverses the polarity of hysteresis loop from clockwise to anticlockwise, indicating T_{com} of Ta/GdFeCo/Cu heterostructures was modulated by the electric field.

To clearly describe electric fields control of T_{com}, temperature dependences of coercivity with unpolarized and electric fields $E = +2.75$ kV cm^{-1} state were extracted and summarized in Fig. 3(a), respectively. Obviously the shift of T_{com} (up to ∼28 K) after applying electric field is observed. The dependences of H_c on temperatures in Fig. 3(a) show three typical regions labeled "I", "II", and "III". The polarity of hysteresis loops is negative (positive) in the region I (III), whereas the change from negative to positive is achieved with applying electric field in the region II, which indicates the change of T_{com} induced by electric field.

To gain insight into the mechanism of the change of T_{com} by electric field, detailed evolution of T_{com} with different electric fields was performed, see Supplemental Material S4 [25] (see also Refs. [30,31] therein) for details. Figure 3(b) displays a typical butterflylike behavior of T_{com}-E curve, which is similar to the behavior of strain-electric field (ϵ-E) curve (blue line) as shown in the inset of Fig. 3(b). It indicates that the modulation of T_{com} by electric field can be attributed to piezostrain-mediated ME coupling in the heterostructures [32–35]. The lack of a pefect match between T_{com}-E and ϵ-E curves could be attributed to domain splitting in the unstaurated PMN-PT ferroelectric substrate [29,36]. Given that the GdFeCo film has a positive magnetostriction coefficient [37], the heterostructures have a positive magnetoelastic anisotropy [29]. By interfacing the GdFeCo film to ferroelecrtric PMN-PT substrate, external electric fields induce in-plane strain in the PMN-PT layer, which is transferred to the magnetic layer (GdFeCo film) and influences the magnetic properties of Ta/GdFeCo/Cu heterostructures. Additionally, the butterflylike behavior clearly demonstrates that there are two distinguishable states at a given electric field, such as at +2.75 kV cm^{-1}. It implies that the history of the applied electric field is important for the modulation. Considering that the heterostructures are thick enough to mitigate the effect of local carrier density, we can safely disregard the charge influence, which results in a typical hysteresislike loop behavior [38–41].

To gain a better underestanding of the piezostrain-mediated ME coupling mechanism, spin-polarized first-principles calculations were performed on a GdFeCo crystal with uniformly distributed Fe and Co atoms in unit cell [see Fig. 4(a)]. The lattice constants were optimized to be $a = 7.135$ Å and $b = c = 7.361$ Å. A slight anisotropy was introduced, which directly

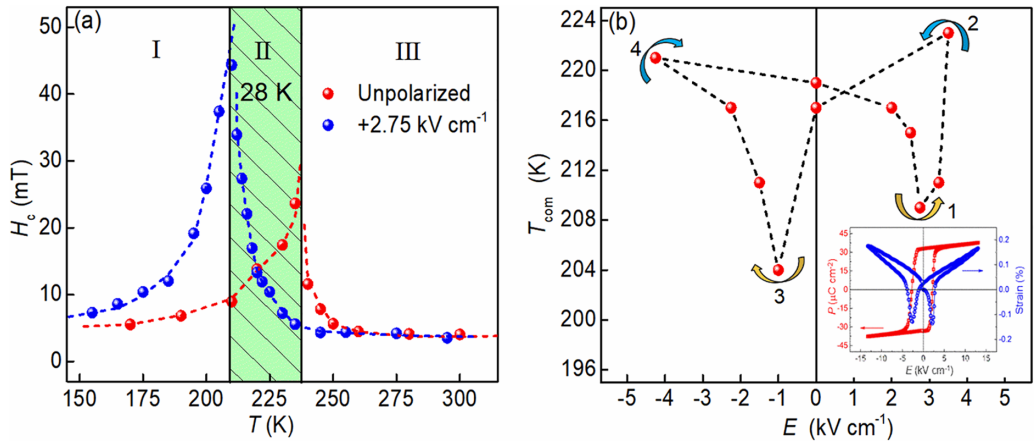

FIG. 3. (a) Coercivity versus temperature in the unpolarized state (red spheres) and at applied electric field of +2.75 kV cm^{-1} (blue spheres). (b) T_{com} under different applied external electric field. The inset shows polarization-electric field (red) and strain-electric field (blue) curves for (011)-oriented PMN-PT substrate at room temperature, which was measured along the (001) direction of PMN-PT substrate.

influnced the bond distances between Gd and Co or Fe atoms. Bond lengths of 2.9746 and 3.0643 Å for the Gd and Fe atoms corresponded to parallel and perpendicular to the x axis bonds, respectively. Similarly, for the Gd and Co atoms, bond lengths of 2.9761 and 3.0224 Å were obtained. The band structure and density of states (DOS) in FIM state are displayed in Fig. 4(b). The bands localized around 8.0 eV below the Fermi level in the spin-down channel are mostly the f orbitals of Gd atoms, while those located around 4.0 eV above the Fermi level also appear in the spin-up channel as well. As a result, Gd atoms have a very large magnetic moment of around 7.47 μ_B. The itinerant d-orbital electrons of Gd atoms contribute about 0.47 μ_B to the total. DOS for the spin-up channel differs from that for the spin down channel near the Fermi level, indicating the appearance of spin splitting. This splitting is primarily defined by the magentic moments of Co and Fe atoms, which are 1.3725 μ_B and 2.3415 μ_B, respectively. The exchange coupling between the Gd, Fe, and Co atoms was calculated in the framework of the Heisenberg model of the exchange for nearest neighbors, the Hamiltonian of which is given by [42]:

$$H = -\sum_{i,\delta} J_{i,i+\delta}\sigma_i\sigma_{i+\delta}.$$

Here, $J_{i,i+\delta}$ is the exchange coupling constant, δ is the number of nearest neighbors, and σ_i is the quantum number of the total spin angular momentum per lattice site, respectively. For simplicity, we assume $J \equiv J_{Gd,Fe} \approx J_{Gd,Co}$ in GdFeCo. Our calculations yield a value of averaged exchange coupling constant J around -4.718 meV, which is comparable to a value of around -5.0 meV for $GdCo_2$ with the same crystal structure [20]. The exchange coupling constantly changes when the uniaxial tensile strain (ϵ) is applied along the x axis: J decreases from -4.7 to -4.8 meV as ϵ increases from 0 to 3%, as shown in Fig. 4(c). The increase in the magnitude of exchange coupling under tensile strain is highly infomative. In fact, we find that the band structure remains nearly unchanged under strain (not provided for brevity). This also holds true for magnetic moments. Under the tensile strain $\epsilon = 3\%$, the bond lengths between the Gd and Co atoms along the x axis increase to 3.0511 Å. The corresponding bond lengths in the direction perpendicular to the x axis however decrease to 3.0060 Å. Noted that the number of bonds perpendicular to the x axis is twice as large as the bonds along the x axis. Similar results are obtained for the Gd and Fe atoms. It is well known that the exchange coupling is closely related to the value of the distance in the exchange integral. The decrease of this distance has a larger effect on the exchange coupling. In detail, the increase of exchange coupling in the direction perpendicular

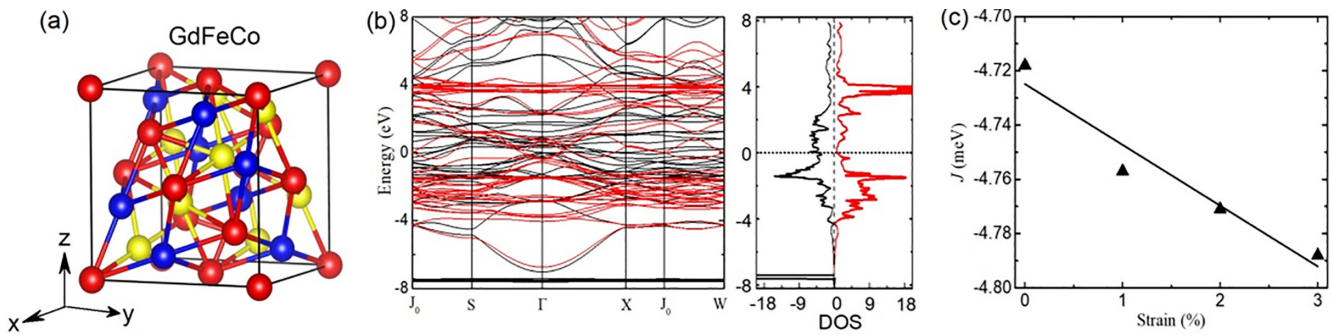

FIG. 4. (a) Crystal structure of GdFeCo. The red, yellow, and blue spheres represent Gd, Fe, and Co atoms, respectively. (b) Calculated band structure and DOS without strain. The red and black lines represent spin up and down channels, respectively. (c) Exchange coupling constant J in GdFeCo as a function of uniaxial tensile strain.

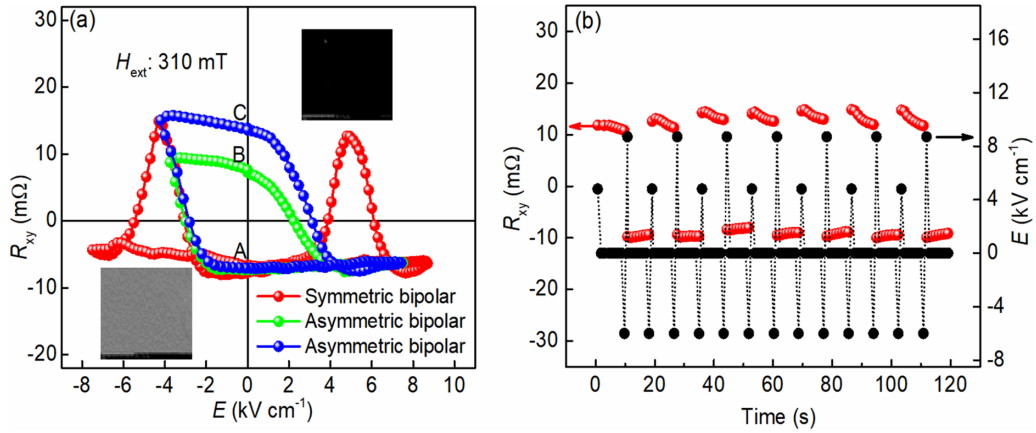

FIG. 5. Nonvolatile ferroelectric switching of resistance in the Cu/GdFeCo/Ta/PMN-PT heterostructures at 214 K. (a) Resistance responses of the heterostructures at the read current of 8 mA under symmetric and asymmetric bipolar sweeping of electric field. Insets show differential wide-field magnetic domain images of the heterostructures. (b) Electric field pulse-induced nonvolatile resistance switching behavior at 214 K, in which a reverse saturation electric field is required during measurements due to the unequal strain in these domain states.

to the tensile strain excessively compensates for the decrease in the direction parallel to the tensile strain, giving rise to an increase in J. While a larger strain was applied in the calculations, the linear relationship between the strain and the value of exchange coupling constant is still satisfied as the strain is less than 0.1%. As a result, the strain-regulated exchange coupling obtained from first-principles calculations agrees with the electric field-regulated T_{com} obtained from experiments. Here, the reason T_{com} should increase is that the Gd moment is supported by exchange to FeCo. Gd on its own has a Curie temperature close to room temperature. The exchange to FeCo maintains the moment in Gd up to and above room temperature. As the exchange increases, the Gd moment at a given temperature increases, causing T_{com} to rise. The theoretical findings allow for a comprehensively understanding of the electric-field-induced butterflylike behavior of T_{com} by an increase in exchange coupling.

B. Nonvolatile resistance switching behavior

Figure 5(a) presents an *in situ* electric field control of saturation R_{xy} at 214 K applying magnetic field 310 mT. The polarities of saturation R_{xy} changing with electric field were observed, which one more again indicates that T_{com} can be controlled by electric fields. To directly describe the effect of electric field on magnetic structure, the images of magnetic domains were obtained by using MOKE after applying symmetric or asymmetric bipolar electric field. As shown in the inset of Fig. 5(a), the gray (measured at "A" point) and the black color (measured at "C" point) correspond to antiparallel and parallel alignment of the FeCo sublattice moment with respect to external field, see Supplemental Material S7 [25] (see also Ref. [43] therein) for details. Additionally, a typical butterflylike behavior of saturation R_{xy} versus electric field (red line) is obtained upon sweeping the symmetric bipolar electric field. This is consistent with the butterflylike ϵ-E curve (blue line) shown in the inset of Fig. 3(b), which indicates the change of the resistance of heterostructures induced by piezostrain. When asymmetric bipolar sweeping was performed, resistance hysteresis loops were achieved that demonstrated the nonvolatile resistance behavior. In particular, difference of resistance was observed once another negative electric field was applied to the piezo-substrate. Therefore, two distinct resistance states at zero electric field were formed: the A state represents the low resistance one and the B (C) state represents the high resistance one, respectively. These results indicate that Ta/GdFeCo/Cu heterostructures exhibit nonvolatile resistance switching behavior.

In order to characterize the repeatability and stability of nonvolatile device according to the potential application requirements. Electric field pulse-induced nonvolatile switching of resistance was measured at 214 K, as shown in Fig. 5(b). Two stable and repeatable resistance states (with opposite polarities) were formated by applying electric field impulses with the duration about 0.5 s. Given the unequal strain in these domain states, a reverse saturation electric field is required during measurements [40]. We label the low and high resistance states as ON and OFF states, respectively. As a result, pulsed electric fields can achieve a repeatable, nonvolatile, and attenuation-free ON and OFF switching, which is suitable for various applications such as amplifiers and trigger devices.

C. Exchange bias behavior regulated by electric field

Based on the above results of electric field control T_{com}, an exchange-biased (EB) device utilizing the magnetic interface effects in antiferromagnetic/ferrimagnetic structure was designed. An antiferromagnetic IrMn layer was deposited on the ferrimagnetic (GdFeCo) layer, inducing the unidirectional exchange coupling effect at the interface between IrMn and GdFeCo [see the inset in Fig. 6(a)]. The temperature-dependent AHE hysteresis loops of the EB device were obtained to confirm the values of T_{com} [11], see Supplemental Material S8 [25] for details. The hysteresis loops at 200 and 225 K, i.e., below and above T_{com} (∼210 K), show apparent EB effect in the device [see Fig. 6(a)]. Figure 6(b) shows temperature dependence of exchange bias field, $H_{eb} = (H_{c+}+H_{c-})/2$. Clearly, H_{eb} increases with decreasing of temperature to T_{com} and changes its sign at T_{com}.

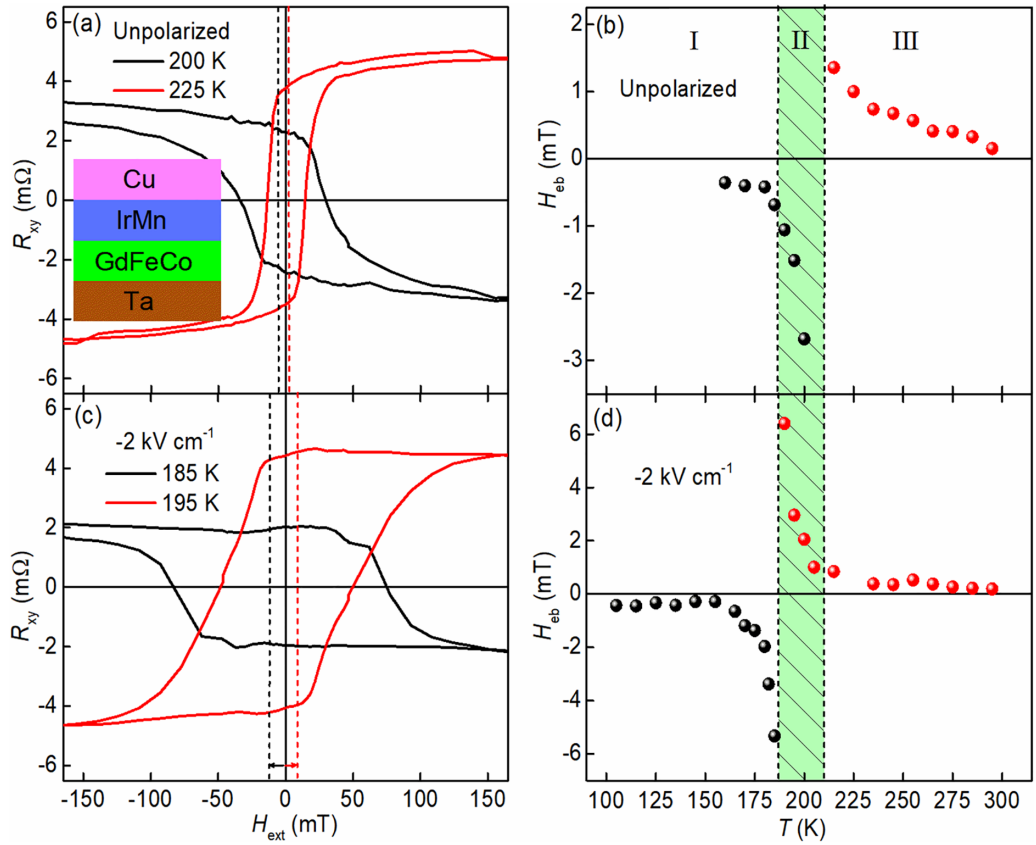

FIG. 6. Electric field control of exchange bias field in the Cu/IrMn/GdFeCo/Ta device. (a) and (c) show, respectively, AHE hysteresis loops of the device in the unpolarized state and at the applied electric field of −C2 kV cm^{-1} at different temperatures. The inset displays schematic illustration of the device layer structure. (b) and (d) show H_{eb} as a function of temperature in the unpolarized state and at the applied electric field of −2 kV cm^{-1}, respectively. The dashed lines in (b) and (d) indicate T_{com} of devices.

Subsequently, the amplitude of H_{eb} starts to decrease and approaches a constant value. Therefore, the bipolar EB effect in our device was obtained [44,45]. Considering that $H_{eb} = \frac{2\sqrt{AK}}{M_{FIM}t_{FIM}}$, where A is the exchange interaction energy, K is the anisotropy constant of IrMn, and M_{FIM} and t_{FIM} are the magnetization and the thickness of FIM film, respectively [14,46,47], our results indicate that pinned spins at GdFeCo/IrMn interface can be reversed by temperature.

Then an electric field was used to control the invert of the net magnetization, which induced the sign change of exchange bias. The temperature dependence of AHE hysteresis loops and coercivity demonstrated that T_{com} of the device decreases to 187 K as the presence of electric field $E = -2$ kV cm^{-1}, see Supplemental Material S9 [25] for details. The hysteresis loops of the device under electric field −2 kV cm^{-1} at the temperatures 185 and 195 K is shown in Fig. 6(c), which show exchange bias effect and the sign change of H_{eb}. Figure 6(d) presents the temperature dependence of H_{eb} with $E = -2$ kV cm^{-1}, which behaves similar to the unpolarized state. In the regions I and III, H_{eb} is negative and positive, respectively, in both the unpolarized and $E = -2$ kV cm^{-1} states. However, in region II, H_{eb} changes from negative to positive after applying electric field $E = -2$ kV cm^{-1}. The obtained results indicate that pinned spins at the interface can be switched by electric field.

D. Nonvolatile exchange bias behavior

Figure 7(a) shows the dependence of H_{eb} in a full electric field cycle at 175 K. A typical butterflylike loop of H_{eb} versus electric field was observed, which is similar to the T_{com}-E and the strain-electric field curves. Noted that the sign change of exchange bias field can be achieved by applying different electric fields. These results show that piezostrain induces the change of T_{com} and net mangetization of ferrimagnetic GdFeCo alloy, which further results in the change of H_{eb} induced by exchange coupling at the interface between IrMn and GdFeCo. To investigate the reversibility and stability of electric field control H_{eb} in our device, an electric field pulse with the duration of approximately 0.5 s was applied at 175 K, as shown in Fig. 7(b). Following the application of pulsed electric field, two stable and reversible EB states (with opposite sign) were observed. This observation points to nonvolatility of the device and confirms that the EB effect is indeed induced by piezostrain-mediated ME coupling in the Cu/IrMn/GdFeCo/Ta/PMN-PT device [48,49]. Obtained effects provide a step forward for the next generation of EB-based devices such as spin valves [50] and hard drive read heads [51], as well as the ability to effectively reduce writing fields in exchange spring media for magnetic storage [52].

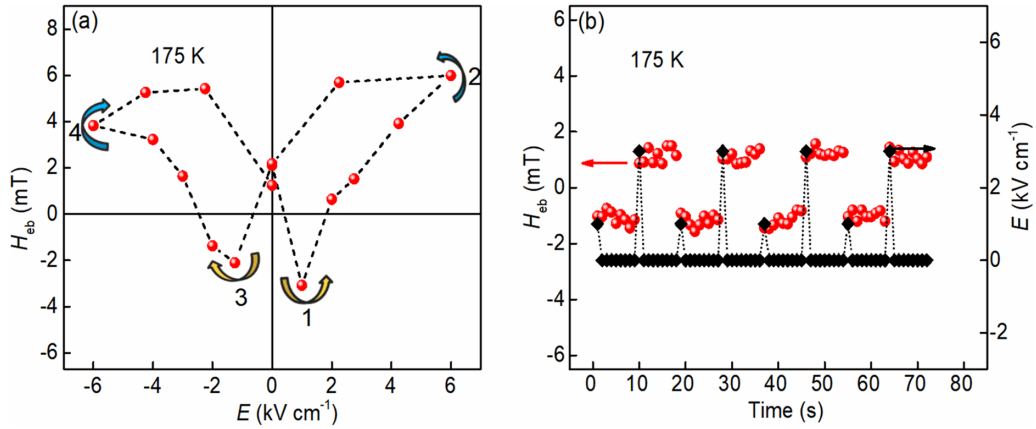

FIG. 7. Electric field dependence of exchange bias field and nonvolatility effect at 175 K. (a) The exchange bias field as a function of the external electric field. The electric field values follow the sequence "1"→ "2" → "3" → "4" which leads to a typical butterflylike curve. (b) The pulsed electric field-induced nonvolatility exchange bias effect.

IV. CONCLUSIONS

In conclusion, we have demonstrated the shift of T_{com} in ferrimagnetic GdFeCo films by applying an electric field across the PMN-PT substrate, indicating electric field control of magnetization. A typical butterflylike curve of T_{com}-E indicates that the change of T_{com} orginates from the piezostrain of the PMN-PT substrate. The spin-polarized first-principles calculations provide a microscopic mechanism for T_{com} modulation based on changes in exchange coupling strength in GdFeCo films by the lattice strain. Nonvolatile and reversible R_{xy} is achieved by pulsed electric fields, which can be used in trigger devices. Furthermore, a nonvolatile bipolar EB-based device with appropriate multilayer design was also fabricated. The results enabled the experimental realization of a piezostrain-induced modulation of T_{com} in ferrimagnetic GdFeCo films. Such piezostrain-controlled magnetization compensation manipulation can be used in energy-efficient solid-state magnetic storage and logic devices.

ACKNOWLEDGMENTS

This work was supported by the Natural Science Foundation of China (Grants No. 52271179, No. 11974149, No. 11874189, No. 12174146, No. 91963201, and No. 11834005), the Natural Science Foundation of Gansu Province (Grant No. 21JR7RA472), the Open Foundation Project of Jiangsu Key Laboratory of Thin Films (Grant No. KJS2036).

APPENDIX: COMPUTATIONAL METHOD

Spin-polarized first-principles calculations were performed using DFT and the projector augmented wave method implemented in the Vienna *ab initio* simulation package (VASP) [53,54]. The exchange-correlation potential was treated using the generalized gradient approximation (GGA) [55] with the Perdew-Burke-Ernzerhof [56] functional corrected for solids. The GGA+U method was applied to the f orbitals of Gd atoms. The value of effective on-site Coulomb interaction parameter was U_{eff}= 6 eV. During the optimization, all atoms were relaxed until the force on each atom was less than 0.01 eV/Å. The conventional unit cell of GdFeCo containing 8 Gd, 8 Fe, and 8 Co atoms was used. A 10 × 10 × 10 k-point mesh and an energy cut-off value of 520 eV were taken. Our calculations showed that GdFeCo had a normal Poisson's ratio.

[1] R. A. Duine, K. J. Lee, S. S. P. Parkin, and M. D. Stiles, Synthetic antiferromagnetic spintronics, Nat. Phys. **14**, 217 (2018).
[2] S. K. Kim, G. S. D. Beach, K. J. Lee, T. Ono, T. Rasing, and H. Yang, Ferrimagnetic spintronics, Nat. Mater. **21**, 24 (2022).
[3] K. J. Kim, S. K. Kim, Y. Hirata, S. H. Oh, T. Tono, D. H. Kim, T. Okuno, W. S. Ham, S. Kim, G. Go, Y. Tserkovnyak, A. Tsukamoto, T. Moriyama, K. J. Lee, and T. Ono, Fast domain wall motion in the vicinity of the angular momentum compensation temperature of ferrimagnets, Nat. Mater. **16**, 1187 (2017).
[4] S. A. Razavi, D. Wu, G. Yu, Y.-C. Lau, K. L. Wong, W. Zhu, C. He, Z. Zhang, J. M. D. Coey, P. Stamenov, P. Khalili Amiri, and K. L. Wang, Joule Heating Effect on Field-Free Magnetization Switching by Spin-Orbit Torque in Exchange-Biased Systems, Phys. Rev. Appl. **7**, 024023 (2017).
[5] M. Wang, Z. Wang, C. Wang, and W. Zhao, Field-free deterministic magnetization switching induced by interlaced spin-orbit torques, ACS Appl. Mater. Interfaces **13**, 20763 (2021).
[6] X. Qiu, P. Deorani, K. Narayanapillai, K. S. Lee, K. J. Lee, H. W. Lee, and H. Yang, Angular and temperature dependence of current induced spin-orbit effective fields in Ta/CoFeB/MgO nanowires, Sci. Rep. **4**, 4491 (2014).
[7] M. Tang, K. Shen, S. Xu, H. Yang, S. Hu, W. Lu, C. Li, M. Li, Z. Yuan, S. J. Pennycook, K. Xia, A. Manchon, S. Zhou, and X. Qiu, Bulk spin torque-driven perpendicular magnetization switching in L_{10} FePt single layer, Adv. Mater. **32**, 2002607 (2020).
[8] X. Zhang, P. X. Qin, Z. X. Feng, H. Yan, X. N. Wang, X. R. Zhou, H. J. Wu, H. Y. Chen, Z. A. Meng, and Z. Q. Liu,

Epitaxial integration of a perpendicularly magnetized ferrimagnetic metal on a ferroelectric oxide for electric-field control, Rare Met. **41**, 1554 (2022).

[9] K. Ueda, M. Mann, P. W. P. de Brouwer, D. Bono, and G. S. D. Beach, Temperature dependence of spin-orbit torques across the magnetic compensation point in a ferrimagnetic TbCo alloy film, Phys. Rev. B **96**, 064410 (2017).

[10] J. A. Gonzalez, J. P. Andres, and R. Lopez Anton, Applied trends in magnetic rare earth/transition metal alloys and multilayers, Sensors **21**, 5615 (2021).

[11] C. Fowley, K. Rode, Y.-C. Lau, N. Thiyagarajah, D. Betto, K. Borisov, G. Atcheson, E. Kampert, Z. Wang, Y. Yuan, S. Zhou, J. Lindner, P. Stamenov, J. M. D. Coey, and A. M. Deac, Magnetocrystalline anisotropy and exchange probed by high-field anomalous Hall effect in fully compensated half-metallic Mn_2Ru_xGa thin films, Phys. Rev. B **98**, 220406(R) (2018).

[12] Z. Zheng, Y. Zhang, V. Lopez Dominguez, L. Sanchez Tejerina, J. Shi, X. Feng, L. Chen, Z. Wang, Z. Zhang, K. Zhang, B. Hong, Y. Xu, Y. Zhang, M. Carpentieri, A. Fert, G. Finocchio, W. Zhao, and P. Khalili Amiri, Field-free spin-orbit torque-induced switching of perpendicular magnetization in a ferrimagnetic layer with a vertical composition gradient, Nat. Commun. **12**, 4555 (2021).

[13] Y. Guo, Y. Wu, Y. Cao, X. Zeng, B. Wang, D. Yang, X. Fan, and J. Cao, The deterministic field-free magnetization switching of perpendicular ferrimagnetic Tb-Co alloy film induced by interfacial spin current, Appl. Phys. Lett. **119**, 032409 (2021).

[14] J. Wang, C. Li, R. Tang, G. Chai, J. Yao, and C. Jiang, Spin-orbit torque in a single ferrimagnetic GdFeCo layer near the compensation temperature, Appl. Phys. Lett. **120**, 102402 (2022).

[15] E. Burzo, L. Chioncel, R. Tetean, and O. Isnard, On the *R* 5*d* band polarization in rare-earth-transition metal compounds, J. Phys.: Condens. Matter **23**, 026001 (2011).

[16] H. Wu, J. Nance, S. A. Razavi, D. Lujan, B. Dai, Y. Liu, H. He, B. Cui, D. Wu, K. Wong, K. Sobotkiewich, X. Li, G. P. Carman, and K. L. Wang, Chiral symmetry breaking for deterministic switching of perpendicular magnetization by spin-orbit torque, Nano Lett. **21**, 515 (2021).

[17] Y. Cao, Y. Sheng, K. W. Edmonds, Y. Ji, H. Zheng, and K. Wang, Deterministic magnetization switching using lateral spin-orbit torque, Adv. Mater. **32**, 1907929 (2020).

[18] Y. W. Oh, S. H. Chris Baek, Y. M. Kim, H. Y. Lee, K. D. Lee, C. G. Yang, E. S. Park, K. S. Lee, K. W. Kim, G. Go, J. R. Jeong, B. C. Min, H. W. Lee, K. J. Lee, and B. G. Park, Field-free switching of perpendicular magnetization through spin-orbit torque in antiferromagnet/ferromagnet/oxide structures, Nat. Nanotechnol. **11**, 878 (2016).

[19] B. J. Chen and G. C. Han, Field-assisted switching of free-layer magnetization in magnetic tunnel junctions, IEEE Magn. Lett. **6**, 6800104 (2015).

[20] M. Huang, M. U. Hasan, K. Klyukin, D. Zhang, D. Lyu, P. Gargiani, M. Valvidares, S. Sheffels, A. Churikova, F. Buttner, J. Zehner, L. Caretta, K. Y. Lee, J. Chang, J. P. Wang, K. Leistner, B. Yildiz, and G. S. D. Beach, Voltage control of ferrimagnetic order and voltage-assisted writing of ferrimagnetic spin textures, Nat. Nanotechnol. **16**, 981 (2021).

[21] W. Hou, A. Azizimanesh, A. Sewaket, T. Pena, C. Watson, M. Liu, H. Askari, and S. M. Wu, Strain-based room-temperature nonvolatile $MoTe_2$ ferroelectric phase change transistor, Nat. Nanotechnol. **14**, 668 (2019).

[22] P. Li, A. Chen, D. Li, Y. Zhao, S. Zhang, L. Yang, Y. Liu, M. Zhu, H. Zhang, and X. Han, Electric field manipulation of magnetization rotation and tunneling magnetoresistance of magnetic tunnel junctions at room temperature, Adv. Mater. **26**, 4320 (2014).

[23] H. Wu, A. Chen, P. Zhang, H. He, J. Nance, C. Guo, J. Sasaki, T. Shirokura, P. N. Hai, B. Fang, S. A. Razavi, K. Wong, Y. Wen, Y. Ma, G. Yu, G. P. Carman, X. Han, X. Zhang, and K. L. Wang, Magnetic memory driven by topological insulators, Nat. Commun. **12**, 6251 (2021).

[24] A. Chen, Y. Zhao, Y. Wen, L. Pan, P. Li, and X. X. Zhang, Full voltage manipulation of the resistance of a magnetic tunnel junction, Sci. Adv. **5**, eaay5141 (2019).

[25] See Supplemental Material S1, S3 and S4 at http://link.aps.org/supplemental/10.1103/PhysRevB.107.184424 for additional details and characterization of Cu/GdFeCo/Ta sample, S2, S5 and S6 for electric-field-controlled polarization current (strain) curves, S7 for polar MOKE hysteresis loops after applying symmetric or asymmetric bipolar electric field, S8 and S9 for AHE hysteresis loops for Cu/IrMn/GdFeCo/Ta sample.

[26] T. Fu, S. Li, X. Feng, Y. Cui, J. Yao, B. Wang, J. Cao, Z. Shi, D. Xue, and X. Fan, Complex anomalous Hall effect of CoGd alloy near the magnetization compensation temperature, Phys. Rev. B **103**, 064432 (2021).

[27] R. C. Bhatt, L.-X. Ye, N. T. Hai, J.-C. Wu, and T.-h. Wu, Spin-flop led peculiar behavior of temperature-dependent anomalous Hall effect in Hf/Gd-Fe-Co, J. Magn. Magn. Mater. **537**, 168196 (2021).

[28] A. Chanda, J. E. Shoup, N. Schulz, D. A. Arena, and H. Srikanth, Tunable competing magnetic anisotropies and spin reconfigurations in ferrimagnetic $Fe_{100-x}Gd_x$ alloy films, Phys. Rev. B **104**, 094404 (2021).

[29] A. Chen, S. Zhang, Y. Wen, H. Huang, J. Kosel, Y. Lu, and X. X. Zhang, Electric-field-enhanced bulk perpendicular magnetic anisotropy in $GdFe/Pb(Mg_{1/3}Nb_{2/3})_{0.7}Ti_{0.3}O_3$ multiferroic heterostructure, ACS Appl. Mater. Interfaces **11**, 47091 (2019).

[30] M. Martini, C. O. Avci, S. Tacchi, C. H. Lambert, and P. Gambardella, Engineering the Spin-Orbit-Torque Efficiency and Magnetic Properties of Tb/Co Ferrimagnetic Multilayers by Stacking Order, Phys. Rev. Appl. **17**, 044056 (2022).

[31] W. Seung Ham, S. Kim, D. H. Kim, K. J. Kim, T. Okuno, H. Yoshikawa, A. Tsukamoto, T. Moriyama, and T. Ono, Temperature dependence of spin-orbit effective fields in Pt/GdFeCo bilayers, Appl. Phys. Lett. **110**, 242405 (2017).

[32] C. Jiang, C. Jia, F. Wang, C. Zhou, and D. Xue, Transformable ferroelectric control of dynamic magnetic permeability, Phys. Rev. B **97**, 060408(R) (2018).

[33] H. Yan, Z. Feng, P. Qin, X. Zhou, H. Guo, X. Wang, H. Chen, X. Zhang, H. Wu, C. Jiang, and Z. Liu, Electric-field-controlled antiferromagnetic spintronic devices, Adv. Mater. **32**, 1905603 (2020).

[34] T. Nan, M. Liu, W. Ren, Z. G. Ye, and N. X. Sun, Voltage control of metal-insulator transition and nonvolatile ferroelastic switching of resistance in VO_x/PMN-PT heterostructures, Sci. Rep. **4**, 5931 (2014).

[35] C. Zhang, F. Wang, C. Dong, C. Gao, C. Jia, C. Jiang, and D. Xue, Electric field mediated nonvolatile tuning magnetism at the single-crystalline $Fe/Pb(Mg_{1/3}Nb_{2/3})_{0.7}Ti_{0.3}O_3$ interface, Nanoscale **7**, 4187 (2015).

[36] L. Yang, Y. Zhao, S. Zhang, P. Li, Y. Gao, Y. Yang, H. Huang, P. Miao, Y. Liu, A. Chen, C. W. Nan, and C. Gao, Bipolar loop-like nonvolatile strain in the (001)-oriented $Pb(Mg_{1/3}Nb_{2/3})O_3$-$PbTiO_3$ single crystals, Sci. Rep. **4**, 4591 (2014).

[37] S. Yoshino, M. Masuda, H. Takahashi, S. Tsunashima, and S. Uchiyama, Magnetostriction of amorphous GdFeCo and YFeCo thin films, J. Appl. Phys. **64**, 5498 (1988).

[38] R. Yu, K. He, Q. Liu, X. Gan, B. Miao, L. Sun, J. Du, H. Cai, X. Wu, M. Wu, and H. Ding, Nonvolatile electric-field control of ferromagnetic resonance and spin pumping in Pt/YIG at room temperature, Adv. Electron. Mater. **5**, 1800663 (2019).

[39] C. Zhou, L. Shen, M. Liu, C. Gao, C. Jia, and C. Jiang, Strong Nonvolatile Magnon-Driven Magnetoelectric Coupling in Single-Crystal $Co/[PbMg_{1/3}Nb_{2/3}O_3]_{0.71}[PbTiO_3]_{0.29}$ Heterostructures, Phys. Rev. Appl. **9**, 014006 (2018).

[40] L. Wu, C. Zhang, C. Dong, C. Jia, C. Jiang, and D. Xue, Polarization-induced resistive switching behaviors in complex oxide heterostructures, Appl. Phys. Lett. **107**, 122905 (2015).

[41] M. Liu, J. Hoffman, J. Wang, J. Zhang, B. Nelson Cheeseman, and A. Bhattacharya, Nonvolatile ferroelastic switching of the Verwey transition and resistivity of epitaxial Fe_3O_4/PMN-PT (011), Sci. Rep. **3**, 1876 (2013).

[42] A. P. Ginsberg, Magnetic exchange in transition metal complexes. Calculation of cluster exchange coupling constants with the X-scattered wave method, J. Am. Chem. Soc. **102**, 111 (1979).

[43] R. Tolley, T. Liu, Y. Xu, S. Le Gall, M. Gottwald, T. Hauet, M. Hehn, F. Montaigne, E. E. Fullerton, and S. Mangin, Generation and manipulation of domain walls using a thermal gradient in a ferrimagnetic TbCo wire, Appl. Phys. Lett. **106**, 242403 (2015).

[44] S. M. Wu, S. A. Cybart, D. Yi, J. M. Parker, R. Ramesh, and R. C. Dynes, Full Electric Control of Exchange Bias, Phys. Rev. Lett. **110**, 067202 (2013).

[45] S. M. Wu, S. A. Cybart, P. Yu, M. D. Rossell, J. X. Zhang, R. Ramesh, and R. C. Dynes, Reversible electric control of exchange bias in a multiferroic field-effect device, Nat. Mater. **9**, 756 (2010).

[46] R. Morales, A. C. Basaran, J. E. Villegas, D. Navas, N. Soriano, B. Mora, C. Redondo, X. Batlle, and I. K. Schuller, Exchange-bias Phenomenon: The Role of the Ferromagnetic Spin Structure, Phys. Rev. Lett. **114**, 097202 (2015).

[47] O. V. Koplak, V. S. Gornakov, Y. P. Kabanov, E. I. Kunitsyna, and I. V. Shashkov, Temperature dependence of the exchange anisotropy of a GdFeCo ferrimagnetic film coupled to the IrMn antiferromagnet, JETP Lett. **109**, 722 (2019).

[48] A. Chen, Y. Zhao, P. Li, X. Zhang, R. Peng, H. Huang, L. Zou, X. Zheng, S. Zhang, P. Miao, Y. Lu, J. Cai, and C. W. Nan, Angular dependence of exchange bias and magnetization reversal controlled by electric-field-induced competing anisotropies, Adv. Mater. **28**, 363 (2016).

[49] G. Zheng, W. Q. Xie, S. Albarakati, M. Algarni, C. Tan, Y. Wang, J. Peng, J. Partridge, L. Farrar, J. Yi, Y. Xiong, M. Tian, Y. J. Zhao, and L. Wang, Gate-tuned Interlayer Coupling in Van Der Waals Ferromagnet Fe_3GeTe_2 Nanoflakes, Phys. Rev. Lett. **125**, 047202 (2020).

[50] M. Bonfim, G. Ghiringhelli, F. Montaigne, S. Pizzini, N. B. Brookes, F. Petroff, J. Vogel, J. Camarero, and A. Fontaine, Element-selective Nanosecond Magnetization Dynamics in Magnetic Heterostructures, Phys. Rev. Lett. **86**, 3646 (2001).

[51] S. Parkin, X. Jiang, C. Kaiser, A. Panchula, K. Roche, and M. Samant, Magnetically engineered spintronic sensors and memory, Proc. IEEE **91**, 661 (2003).

[52] D. Suess, T. Schrefl, S. Fähler, M. Kirschner, G. Hrkac, F. Dorfbauer, and J. Fidler, Exchange spring media for perpendicular recording, Appl. Phys. Lett. **87**, 012504 (2005).

[53] G. Kresse and J. Furthmuller, Efficiency of *ab initio* total energy calculations for metals and semiconductors using a plane-wave basis set, Comput. Mater. Sci. **6**, 15 (1996).

[54] G. Kresse and J. Hafner, *Ab initio* molecular dynamics for liquid metals, Phys. Rev. B **47**, 558 (1993).

[55] K. Burke, J. Perdew, and M. Ernzerhof, Why the generalized gradient approximation works and how to go beyond it, Int. J. Quantum Chem. **61**, 287 (1997).

[56] B. Hammer, L. B. Hansen, and J. K. Norskov, Improved adsorption energetics within density-functional theory using revised Perdew-Burke-Ernzerhof functionals, Phys. Rev. B **59**, 7413 (1999).